Applied Catalysis B: Environmental 343 (2024) 123508

Contents lists available at ScienceDirect

Applied Catalysis B: Environmental

journal homepage: www.elsevier.com/locate/apcatb

Revealing the effect of metal-support interactions at the Ni/In_2O_3(111) interface on the selective CO_2 hydrogenation

Yishui Ding [a,b,1], Jie Chen [a,c,1], Xu Lian [b,1], Zhangliu Tian [b], Xiangrui Geng [b], Yihe Wang [a,b], Yuan Liu [a,b], Wei Wang [a,b], Meng Wang [a,b], Yukun Xiao [a,b], Tengyu Jin [c], Mingyue Sun [a,b], Zhenni Yang [d], Kelvin H.L. Zhang [d], Jian-Qiang Zhong [e,*], Wei Chen [a,b,c,f,**]

[a] Joint School of National University of Singapore and Tianjin University, International Campus of Tianjin University, Binhai New City, Fuzhou 350207, PR China
[b] Department of Chemistry, National University of Singapore, 3 Science Drive 3, 117543, Singapore
[c] Department of Physics, National University of Singapore, 2 Science Drive 3, 117542, Singapore
[d] College of Chemistry and Chemical Engineering, Xiamen University, Xiamen 361005, PR China
[e] School of Physics, Hangzhou Normal University, No. 2318, Yuhangtang Road, Hangzhou 311121, Zhejiang, PR China
[f] National University of Singapore (Suzhou) Research Institute, 377 Lin Quan Street, Suzhou 215123, PR China

ARTICLE INFO

Keywords:
CO_2 hydrogenation
Indium oxide
Nickel
Metal-support interaction
In-situ NAP-XPS

ABSTRACT

In_2O_3-supported Ni catalysts exhibit remarkable catalytic activity and selectivity in CO_2 hydrogenation to methanol, but the underlying mechanisms and metal-oxide interactions during the reaction remain elusive. Herein, we investigate the Ni-In_2O_3 interaction by physical vapor deposition of Ni onto well-defined In_2O_3(111) thin films. In-situ near ambient-pressure X-ray photoelectron spectroscopy (NAP-XPS) was employed to probe the CO_2 hydrogenation processes on these Ni/In_2O_3(111) model systems. Our results reveal that the small Ni clusters supported on the In_2O_3(111) surface at low Ni coverages exhibit cationic states. The chemical bonding and associated electron transfer at the Ni/In_2O_3(111) interface play crucial roles in the activation of H_2 and CO_2. Importantly, reaction intermediates (CO_3*, OH, and HCOO*) are readily formed and desorbed under CO_2 hydrogenation conditions. Our study highlights the significance of metal-support interactions on the selectivity of CO_2 hydrogenation. These findings provide valuable insights into the rational design of advanced In_2O_3-based catalysts for CO_2 hydrogenation.

1. Introduction

The excessive consumption of fossil fuels has led to a significant rise in carbon dioxide (CO_2) emissions, which are associated with environmental concerns such as climate change, sea-level rise, and seawater acidification [1–3]. To address these issues, a promising strategy is to establish a sustainable carbon cycle that involves capturing CO_2 emissions from fossil fuel combustion processes and converting them into value-added chemicals [4–6]. One of the most attractive options is the catalytic conversion of CO_2 with renewable energy-generated hydrogen (H_2) to methanol (CH_3OH), which can serve as an energy carrier and be transformed into valuable fuel alternatives and chemicals [7–9]. However, the catalytic hydrogenation of CO_2 to CH_3OH still presents challenges, including poor selectivity, the lack of stable catalysts, and controversial reaction mechanisms [10–13].

The hydrogenation of CO_2 to methanol is a thermodynamically favorable process, particularly at moderate temperatures of 473–573 K and pressures of 40–100 bar [14]. The copper (Cu)-based catalysts, industrial employed for methanol synthesis from syngas, have been extensively investigated for CO_2 conversion to methanol. Nevertheless, these catalysts suffer from low methanol selectivity due to their significant involvement in the competing reverse water-gas shift reaction (RWGS) and the rapid deactivation of the Cu component [15,16]. This limitation highlights the urgent need for the development of catalysts with improved activity, selectivity, and long-term stability for efficient CO_2-to-methanol conversion. Encouragingly, indium oxide (In_2O_3) has

* Corresponding author.
** Corresponding author at: Joint School of National University of Singapore and Tianjin University, International Campus of Tianjin University, Binhai New City, Fuzhou 350207, PR China.
E-mail addresses: zhong@hznu.edu.cn (J.-Q. Zhong), phycw@nus.edu.sg (W. Chen).
[1] These authors contributed equally.

https://doi.org/10.1016/j.apcatb.2023.123508
Received 26 June 2023; Received in revised form 7 November 2023; Accepted 10 November 2023
Available online 14 November 2023

garnered particular interest as a catalytic material due to its exceptional methanol selectivity (up to 100%) and higher activity as compared to the conventional $Cu/ZnO/Al_2O_3$ catalyst in CO_2 hydrogenation [17–19]. Density functional theory (DFT) studies have highlighted the significance of oxygen vacancies (O_v) on the catalyst surface in facilitating CO_2 activation and hydrogenation by stabilizing essential intermediates during catalytic reactions [20–22]. However, despite its high selectivity for direct CO_2 conversion to CH_3OH, In_2O_3 exhibits poor H_2-splitting ability, constraining the overall CO_2 conversion rate. Incorporating metal promoters such as Pd [23–25], Ni [26–28], Pt [29,30], Rh [31,32], Au [33], Re [34], etc., known for efficient hydrogen dissociation, into the oxide has significantly enhanced catalytic performance in the selective hydrogenation of CO_2 to CH_3OH. Previous studies have indicated that a strong interaction between In_2O_3 and metal promoters, along with modulation of the electronic properties of the metal, can generate additional active metal/In_2O_3 interfacial sites to accelerate methanol production [35–37].

In_2O_3-supported Ni catalysts have emerged as a promising option due to their relative cost-effectiveness and superior catalytic performance compared to intrinsic In_2O_3 catalysts. Frei et al. [26] found that highly dispersed $InNi_3$ alloy phases on the oxide surface contribute to the homolytic splitting of hydrogen. Conversely, small Ni clusters were active in the RWGS reaction. Snider et al. [38] demonstrated that bimetallic Ni-In catalysts exhibited improved catalytic activity and selectivity towards methanol, attributed to the synergistic effects between the Ni-In alloy and oxide components. In contrast to the previously reported Ni-In alloyed catalysts, Jia et al. [28] noted that highly dispersed Ni species, which strongly interact with In_2O_3, exhibited a promoting effect on the selective CO_2 hydrogenation to CH_3OH without CH_4 formation. Moreover, Zhu et al. [27] suggested that the higher activity of NiO/In_2O_3 catalysts for CH_3OH synthesis is due to the low-barrier H_2 dissociation on reduced Ni in the form of single atoms and clusters during CO_2 hydrogenation, facilitating the hydrogenation of adsorbed CO_2 on O_v. Similar arguments have been made regarding the active site in other metal promoter catalysts (Pd, Cu, etc.) within In_2O_3 catalytic systems [24,39–41]. These arguments regarding active site identification have often arisen from complex catalyst systems, ex-situ characterizations and reliance on DFT calculations. Therefore, the need for experimental evidence describing the in-situ evolution of reaction intermediates and metal-support interactions during CO_2 hydrogenation is crucial for a comprehensive understanding of the catalytic process. With respect to this, "surface science" investigations employing surface-sensitive techniques on model catalysts have the potential to elucidate the surface chemistry of Ni/In_2O_3-based catalysts and shed light on the promotional effects of Ni in CO_2 hydrogenation processes [42–44].

To comprehensively understand the Ni-In_2O_3 interaction under CO_2 hydrogenation-relevant conditions, we employ well-defined model systems by physical vapor deposition of Ni onto the $In_2O_3(111)$ surface in this work. Indeed, the (111) facet of In_2O_3 is intentionally chosen for its non-polar nature and high thermodynamic stability [20,45]. We investigate the surface chemistry of Ni/$In_2O_3(111)$ model catalysts upon exposure to CO_2, H_2, and CO_2/H_2 mixtures at temperatures ranging from 300 to 673 K using near-ambient pressure X-ray photoelectron spectroscopy (NAP-XPS), ultraviolet photoelectron spectroscopy (UPS), and low-energy electron diffraction (LEED). Our results demonstrate that Ni/$In_2O_3(111)$ model catalysts with low Ni coverages possess unique chemical and structural properties. Specifically, we observe the presence of small-sized Ni clusters that induce electronic perturbations in chemisorbed cationic Ni atoms located directly at the Ni−In_2O_3 interface, thus promoting the activation of H_2 and CO_2. The oxygen vacancies generated on the reduced $In_2O_3(111)$ support under CO_2 hydrogenation conditions greatly enhance the activation of the C-O bonds. Intriguingly, the hydrogenation of adsorbed CO_3* to formate (HCOO*) is observed upon adding H_2, thus supporting the HCOO* pathway for selective CH_3OH generation as demonstrated in previous theoretical calculations. Conversely, the Ni/$In_2O_3(111)$ surface with a higher Ni coverage possesses a weakened metal-oxide interaction, leading to the formation of CO and atomic carbon intermediates and resulting in distinctly different reaction paths during CO_2 hydrogenation.

2. Experimental

A 200 nm $In_2O_3(111)$ thin film was fabricated on a Y-$ZrO_2(111)$ substrate with atomically flat surfaces by using pulsed laser deposition (PLD) [46–48]. The deposition process for the $In_2O_3(111)$ film was conducted at 923 K under an oxygen partial pressure of 1.33 Pa. Subsequently, the $In_2O_3(111)$ sample was mounted on a Mo sample holder using Ta strips and loaded into an ultrahigh-vacuum (UHV) system. The setup consists of a homemade preparation chamber and a lab-based SPECS NAP-XPS/UPS analysis chamber, as detailed in our previous works [49–52].

The $In_2O_3(111)$ thin film was cleaned via several cycles of Ar^+ sputtering (500 V, 6 μA) for 10 min and subsequently annealed in 3×10^{-7} mbar O_2 at 773 K for 20 min. The as-prepared $In_2O_3(111)$ thin film shows a well-resolved hexagonal LEED pattern without adventitious carbon as evidenced in the XPS C 1 s spectra. The preparation method effectively reduced surface defects and islands, which resulted in a stoichiometric $In_2O_3(111)$ film [53]. To prepare the Ni/$In_2O_3(111)$ model system, Ni (99.98%, Alfa Aesar) was deposited onto the clean $In_2O_3(111)$ surface at 300 K using a Focus EFM3 e-beam evaporator. The Ni deposition rate was ~0.05 monolayer (ML)/min. The nominal Ni coverages were obtained from the INFICON quartz crystal microbalance (QCM) measurements, as well as from the estimations based on the attenuation of the In 3d XPS signal.

During the NAP-XPS experiments, high-purity CO_2 (99.9%) and H_2 (99.999%) gases were introduced into the NAP cell through separate gas lines. The gas flow was controlled using high-precision leak valves and monitored with a Pirani Vacuum cold cathode full-range gauge. The reaction gas was initially introduced at 300 K and then the temperature was increased stepwise up to 673 K. Before the NAP-XPS measurements, the samples were kept at the predetermined pressure and temperature for 15 min, ensuring a relatively steady-state surface condition. The UPS spectra were recorded before and after transferring the sample outside the NAP cell using a He I ($h\nu$ = 21.2 eV) UV source. The sample was biased with −7 V to distinguish the secondary electron cutoff (SECO) from the low kinetic energy electron region.

The XPS core-level spectra of In 3d, In MNN, O 1 s, C 1 s, and Ni $2p_{3/2}$ were acquired using Al Kα radiation ($h\nu$ = 1486.61 eV). The Ag 3d peak at 368.2 eV of a sputter-cleaned Ag(111) sample was used for binding energy calibration. The energy resolution of the instrument was estimated to be about 1.0 eV (the full width at half maximum of the Ag $3d_{3/2}$ peak). The core-level peaks were analyzed using CasaXPS with the subtraction of a Shirley-type background. The GL(30) line shape (70% Gaussian and 30% Lorentzian) was used to fit collected O 1 s and C 1 s spectra. To minimize variations in absolute intensities among experiments, the In MNN Auger peaks were normalized by the background level of a pristine surface under a UHV environment.

3. Results and discussion

3.1. The interaction between Ni/$In_2O_3(111)$ and CO_2

The interaction of Ni with $In_2O_3(111)$ surfaces, as well as CO_2 activation on $In_2O_3(111)$ and Ni/$In_2O_3(111)$ surfaces were first examined. Fig. 1a displays valence band (VB) spectra of pristine and Ni-deposited $In_2O_3(111)$ surfaces. The $In_2O_3(111)$ surface exhibits an O 2p dominated VB structure at 4.0 eV with negligible band gap states below the Fermi level (E_f), consistent with previous reports [46,48]. Upon depositing 0.15 ML Ni on the $In_2O_3(111)$ surface at 300 K, occupied Ni 3d states appeared between 3 and 1 eV in the VB region [54,55]. Such low density of states (DOS) around the E_f indicates that there are strong

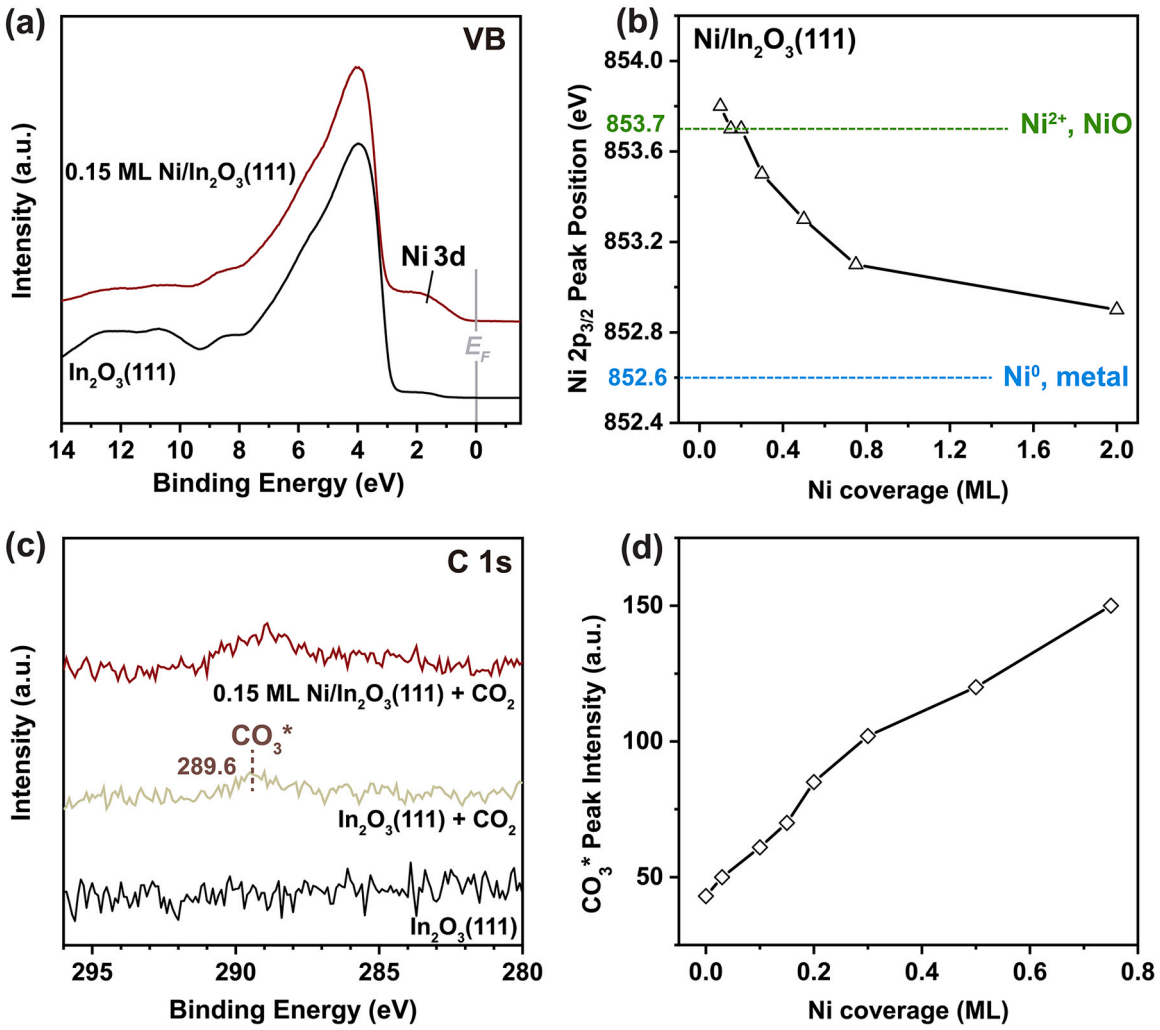

Fig. 1. (a) UPS spectra of the VB region for the pristine $In_2O_3(111)$ and 0.15 ML Ni/ $In_2O_3(111)$ surfaces. (b) The binding energy positions of Ni $2p_{3/2}$ peak as a function of the Ni coverage (θ_{Ni}) on the $In_2O_3(111)$ surface. The lines at 853.7 and 852.6 eV correspond to bulk NiO and metallic Ni references, respectively. (c) XPS spectra of the C 1 s region collected after exposing to 0.2 mbar CO_2 on the $In_2O_3(111)$ and 0.15 ML $Ni/In_2O_3(111)$ surfaces at 300 K. (d) The signal intensities for adsorbed CO_3* species in the C 1 s region as a function of θ_{Ni} on $Ni/In_2O_3(111)$.

electronic perturbations upon the Ni atoms adsorptions, which are essential to the structural, chemical, and catalytic properties at the $Ni/In_2O_3(111)$ interface [56–58]. Additionally, the surface structures of both surfaces were examined using LEED measurements, as depicted in Fig. S1. After depositing 0.15 ML of Ni, the LEED pattern remains unchanged, i.e., the (1 × 1) reflections correspond to the reciprocal lattice vectors of the $In_2O_3(111)$ surface [45,47].

We also investigated the chemical state of Ni on $In_2O_3(111)$ surfaces by monitoring the Ni $2p_{3/2}$ XPS spectra at different coverages (Fig. S2a). As shown in Fig. 1b, with a small amount deposition of Ni (θ_{Ni} ~0.15 ML) on the $In_2O_3(111)$ surface, the Ni $2p_{3/2}$ peak appears at 853.7 eV, indicating cationic Ni adatoms in direct contact with oxide support, which can be attributed to strong metal-support interactions. Additionally, a decrease in the work function (Fig. S2b) and a weak downward band bending effect (Fig. S2c) suggest surface electron transfer from Ni to the $In_2O_3(111)$ support [59]. As the Ni coverage exceeds 0.3 ML, the characteristic features of metallic Ni start to emerge, indicating the growth of three-dimensional (3D) Ni particles [60,61]. Wagner et al. [62] have studied the growth mode of vapor-deposited Fe on the $In_2O_3(111)$ surface at 300 K using Scanning tunneling microscopy (STM) and XPS. They observed that upon depositing 0.28 ML of Fe, highly dispersed Fe adatoms (small clusters) were formed with oxidized Fe^{3+} states. With increasing coverage, the adatoms became disordered, eventually forming large clusters and 3D particles, accompanied by a lower oxidation state of Fe. Based on thermodynamic data, they inferred that other elements (such as Ni or Co) are likely to exhibit similar growth behavior on the oxide surface. Hence, it can be speculated that on the $In_2O_3(111)$ surface, the cationic Ni adatoms in contact with the In_2O_3 surface will induce electronic perturbations at the Ni/In_2O_3 interfaces. As we will discuss below, the strong bonding between Ni and In_2O_3, as well as the electron transfer occurring at the Ni/In_2O_3 interface significantly alter the reactivity of the system during CO_2 hydrogenation.

In Fig. 1c, the C 1 s XPS spectra compare the pristine $In_2O_3(111)$ and 0.15 ML $Ni/In_2O_3(111)$ surfaces after exposure to 0.2 mbar CO_2 at 300 K. The peak at around 288–290 eV in the C 1 s region for both surfaces appears following CO_2 exposure, which is assigned to the adsorbed CO_3* species [63–65]. On the $In_2O_3(111)$ surface, the peak at 289.6 eV corresponds to CO_3* species formed by the direct reaction of CO_2 with surface O atoms [21,66,67]. The intensity of CO_3* species on the $Ni/In_2O_3(111)$ surface is much stronger (by 1.6 times), accompanied by a broadening of the CO_3* peak and a slight shift towards lower binding energies. These phenomena are likely associated with the emergence of $NiCO_3$ facilitated by CO_2 adsorption on additional interfacial sites at cationic Ni sites, as inferred from the Ni $2p_{3/2}$ spectra (Fig. S3b). Remarkably, the adsorbed CO_3* peak remains observable on the $Ni/In_2O_3(111)$ surface even at 673 K (Fig. S3a). Fig. 1d illustrates the

intensity of CO_3* peak as a function of Ni coverage on the In_2O_3(111) surface after exposure to CO_2 at 300 K. It should be noted that although the electronic perturbations decrease at the Ni/In_2O_3 interfaces with higher Ni coverages (> 0.3 ML), the amount of adsorbed CO_3* species still increases.

The VB spectra of Ni/In_2O_3(111) surfaces were measured before and after CO_2 exposure (Fig. S4). Following gas exposure, a pronounced attenuation of the Ni 3d states is observed, accompanied by the emergence of CO_3* features [68,69]. The intensities of these CO_3* peaks increase with higher Ni coverage, in line with the observations in Fig. 1d. Nevertheless, it cannot be excluded that CO_2 dissociation ($CO_2 \rightarrow CO_{ads} + O_{ads}$) occurs on the metallic Ni states, followed by further reaction of CO_2 with atomic oxygen to form CO_3* species [64,70,71]. Our experimental results show that CO_2 only weakly chemisorbs on the O sites of the In_2O_3(111) surface. In contrast, the addition of Ni onto the In_2O_3(111) surface enhances CO_2 adsorption, suggesting that the Ni/In_2O_3(111) surfaces have additional active sites for CO_2 adsorptions and CO_3* stabilizations.

3.2. Formation of oxygen vacancies on Ni/In_2O_3(111) under H_2 reduction

Fig. 2 presents the NAP-XPS spectra of O 1 s, Ni $2p_{3/2}$, and In MNN regions during the exposure of a Ni/In_2O_3(111) surface (θ_{Ni} ~0.15 ML) to 0.2 mbar H_2 at elevated temperatures. In Fig. 2a, the O 1 s spectrum of the pristine Ni/In_2O_3(111) surface shows a main peak at 530.4 eV, along with a shoulder at 532.2 eV, originating from lattice oxide (In-O) and surface hydroxyls (OH) groups, respectively. The presence of intrinsic OH groups can be explained by the dissociative adsorption of water from the UHV background [72]. Upon introducing H_2 into the system at 300 K, the concentration of OH species increases due to the dissociative adsorption of H_2 on the surface. Fig. 2b shows a notable shift to higher binding energies in the Ni $2p_{3/2}$ peak, suggesting the presence of the Ni (OH)-related component at the Ni/In_2O_3(111) interface [73]. Interestingly, the In MNN Auger spectrum remains unaffected by H_2 dissociation at 300 K (Fig. 2c). As the temperature ramps up to 573 K, the signal intensity of surface OH groups decreases, indicating the desorption of OH species. Simultaneously, the Ni $2p_{3/2}$ XPS spectrum reveals a partial reduction of the Ni clusters from Ni^{2+} to Ni^0, as evidenced by the appearance of the Ni $2p_{3/2}$ peak at a lower binding energy (852.9 eV). At 673 K, the Ni^{2+} species undergo further reduction to Ni^0, accompanied by a partial reduction of the In_2O_3(111) surface due to the formation of lattice O_v. As a comparison, the dissociation of H_2 on In_2O_3(111) is negligible (Fig. S5), where the oxidation state of the In^{3+} cations remains unchanged under H_2 reduction. Therefore, the addition of Ni facilitates the H_2 activation at the Ni/In_2O_3 interface and leads to an increase in the surface O_v concentration [27,28,36,74].

XPS measurements of the O 1 s core-level binding energies have been widely employed in various studies to estimate the percentage of O_v and to establish a correlation with its surface catalytic activity [17,24,27,36]. The shoulder peak observed at 531–532 eV in the O 1 s spectrum is commonly attributed to oxygen atoms near or adsorbed on the O_v in metal oxides [75]. However, the estimation of the vacancy concentration based on O 1 s spectra can be challenging, especially for practical catalysts that have been exposed to air before XPS measurements, as signals from surface adventitious hydroxyl and hydrocarbon species cannot be avoided. In the H_2 reduction of Ni/In_2O_3(111), the appearance of In_2O_{3-x} leads to a decrease in the intensity of the shoulder peak at 532 eV in the O 1 s spectrum (Fig. 2a). Theoretical calculations have suggested that the formation of O_v has a negligible impact on the O 1 s core-level shift. Furthermore, it is also difficult to distinguish the contributions from different types of OH groups and O_v compositions in the O 1 s region [76,77]. Therefore, the assignment of the shoulder peak in the O 1 s spectra should be very careful and further studies are needed. Nevertheless, the formation of O_v on Ni/In_2O_3(111) under H_2 reduction is conclusive, which is essential for selective CO_2 hydrogenation.

3.3. Surface chemistry of CO_2 hydrogenation on Ni/In_2O_3(111)

The reaction intermediates and metal-support interactions involved in the CO_2 hydrogenation process on Ni/In_2O_3(111) systems were examined using NAP-XPS and UPS. Fig. 3a-c present the NAP-XPS spectra of the C 1 s, Ni $2p_{3/2}$, and In MNN regions, respectively. The as-prepared Ni/In_2O_3(111) surface with ~0.15 ML of Ni was exposed to 0.6 mbar H_2 and 0.2 mbar CO_2 at elevated temperatures. At 300 K, a peak centered at 290.0 eV emerged in the C 1 s region (Fig. 3a), which can be ascribed to CO_3* and formate (HCOO*) species (Fig. S3a) [78,79]. The presence of HCOO* species was confirmed by the UPS spectra in Fig. 3d, which exhibit four characteristic peaks at 5.3 eV, 9.0 eV, 11.6 eV, and 14.2 eV after exposing to the CO_2/H_2 mixtures [69,80]. These results indicate that the adsorbed CO_3* was hydrogenated into HCOO* on the surface, supporting the theoretical calculations of the HCOO* pathway for CH_3OH production [20,21,74,81]. In addition, the intensity of the O 1 s peak shoulder increases under CO_2 hydrogenation

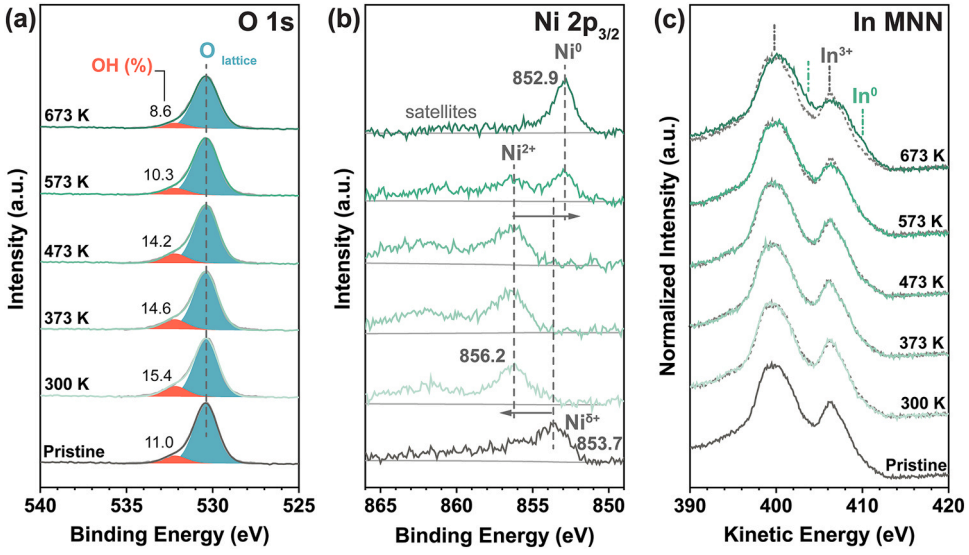

Fig. 2. NAP-XPS spectra for the Ni/In_2O_3(111) surface (θ_{Ni} ~0.15 ML) under 0.2 mbar H_2 at elevated temperatures. (a) O 1 s, (b) Ni $2p_{3/2}$, and (c) In MNN. The gray dashed lines correspond to the pristine Ni/In_2O_3(111) surface. The number shown in (a) represents the area percentage of the fitted OH in O 1 s peak (%).

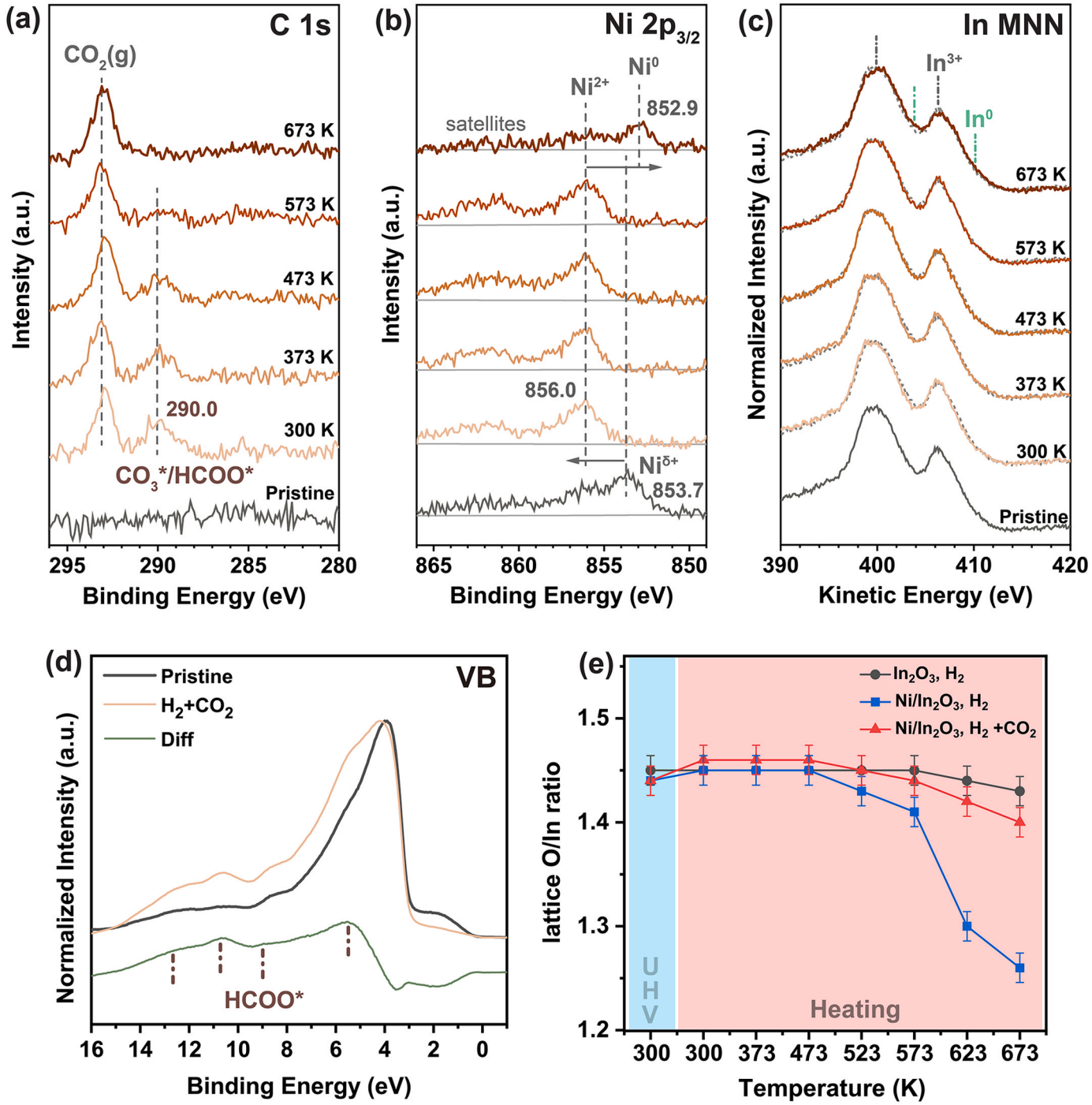

Fig. 3. NAP-XPS spectra for the Ni/In_2O_3(111) surface (θ_{Ni} ~0.15 ML) under 0.6 mbar H_2 + 0.2 mbar CO_2 at the indicated temperatures. (a) C 1 s, (b) Ni $2p_{3/2}$, and (c) In MNN. The gray dashed lines correspond to the pristine Ni/In_2O_3(111) surface. (d) Normalized UPS spectra of VB region for Ni/In_2O_3(111) (θ_{Ni} ~0.15 ML) surface before and after exposing to H_2/CO_2 mixtures at 300 K. The green spectrum depicts the differences between the gas-exposed surface and the pristine surface. (e) The ratio between the lattice O and In as calculated from the O 1 s ($O_{lattice}$) and the In 3d signals.

conditions due to the formation of HCOO* and CO_3* species (Fig. S6). These reaction intermediates exhibit relatively low thermal stability, gradually decreasing as the surface was heated to 573 K. At 673 K, the HCOO* and CO_3* species completely desorbed, leaving only a small concentration of OH groups on the surface. In contrast, the CO_3* species generated from pure CO_2 adsorption remains even at 673 K (Fig. S3a). Thus, these reaction intermediates can be easily formed and transformed on Ni/In_2O_3(111) surface under CO_2 hydrogenation, and no carbon deposition occurs during the reaction.

Within the temperature interval of 300–573 K, the Ni $2p_{3/2}$ peak (Fig. 3b) shifts towards higher binding energy during CO_2 hydrogenation, indicating oxidation of the Ni clusters. At 673 K, partial reduction of Ni^{2+} cations to the metallic state is observed, but no significant evidence of $In^{3+} \rightarrow In^0$ reduction is detected in the In MNN spectra (Fig. 3c). As discussed earlier, the H_2 reduction can induce the reduction of the In_2O_3 support (Fig. 2c). However, during CO_2 hydrogenation with H_2, the reduced In_2O_{3-x} support can be quickly re-oxidized to In_2O_3, suggesting the establishment of a balanced redox cycle within the Ni/In_2O_3(111) system during CO_2 hydrogenation conditions [22,82].

We quantified the mole ratio of lattice O/In ($R_{O/In}$) for In_2O_3(111)

and Ni/In_2O_3(111) surfaces (θ_{Ni} ~0.15 ML) under different reaction conditions using Scofield-derived relative sensitivity factors (RSF) [33,83]. As shown in Fig. 3e, the $R_{O/In}$ is similar below the temperature of 473 K (~ 1.45). Under a pure H_2 atmosphere, the $R_{O/In}$ of In_2O_3(111) remains stable because of the limited capacity for H_2 dissociation on this surface. However, on Ni/In_2O_3(111), the $R_{O/In}$ gradually decreases from a reaction temperature of 523 K and reaches 1.25 at 673 K. The decrease signifies the depletion of O in the In_2O_3 support. In contrast, the $R_{O/In}$ remains relatively stable even at 573 K under a mixed CO_2/H_2 atmosphere, suggesting that O_v can be replenished through CO_2 adsorption, accompanied by the formation of CO_3* and HCOO* intermediates. These in-situ NAP-XPS results offer direct experimental evidence that oxygen vacancies play a crucial role in the activation of CO_2 during CO_2 hydrogenation.

3.4. Effect of Ni coverage on In_2O_3(111) for CO_2 hydrogenation

In addition to investigating the adsorption properties at lower Ni coverage regimes, it is also worthwhile to examine the hydrogenation behavior at higher Ni coverages, where collective phenomena can lead to a complete understanding of the metal-support interaction [57]. In this respect, we explored the impact of increased Ni coverage on the performance of the Ni/In_2O_3(111) surface during CO_2 hydrogenation. Fig. 4 displays the NAP-XPS spectra of the C 1 s, Ni $2p_{3/2}$, and In MNN regions obtained from the Ni/In_2O_3(111) surface (θ_{Ni} ~0.50 ML) under CO_2/H_2 mixtures at elevated temperatures. At 300 K, the C 1 s spectra (Fig. 4a) show a CO_x peak at 289.8 eV probably originating from adsorbed HCOO* and CO_3* species. However, with the rising temperature up to 473 K, the intensity of the CO_x peak slightly decreases, accompanied by the emergence of two new peaks at 286.1 eV and 283.8 eV. The peak at 286.1 eV can be attributed to the adsorption of CO on the Ni sites, as supported by a reference experiment presented in the Supplementary material (Fig. S7) [84,85]. The component at 283.8 eV corresponds to atomic carbon (C_{atomic}) [64,71]. As the temperature rises to 573 K, the CO_x signal is strongly attenuated, while the signals for CO and C_{atomic} become more pronounced. Similar evolutions have been observed during CO_2 reduction on Ni(111) surfaces [64]. The generation of C_{atomic} is believed to be a consequence of CO_x decomposition. Adsorbed CO species can be served as a potential source for the C_{atomic} on metallic Ni [86], which is evident at 673 K, as indicated by the simultaneous weakening of the CO signal and enhancement of the C_{atomic} peak. The presence of CO on the Ni/In_2O_3(111) surface indicates the occurrence of the RWGS reaction ($CO_2 + H_2 \rightarrow CO + H_2O$), while C_{atomic} is likely a precursor for CH_4 formation in CO_2 methanation ($CO_2 + 4\ H_2 \rightarrow CH_4 + 2\ H_2O$) [87]. These findings are consistent with previous studies on practical Ni/In_2O_3 catalysts, which have been demonstrated that low Ni loadings can promote CH_3OH formation, while higher Ni loadings result in the formation of CO and CH_4 [27,28].

As mentioned earlier, on 0.15 ML Ni/In_2O_3(111) surface, the metallic Ni species was only observed at a high temperature of 673 K under H_2/CO_2 mixtures. However, when the Ni coverage is increased to 0.5 ML, the surface becomes more susceptible to reduction. As shown in Fig. 4b, the metallic Ni species start to appear at 473 K and significantly increase at the temperature of 573–673 K. Meanwhile, the In MNN spectrum (Fig. 4c) shows clear evidence of metallic In^0 at 673 K. These observations indicate relatively weaker interactions for larger Ni clusters with In_2O_3(111) support [88].

4. Discussions

Previous experimental and DFT studies have investigated the effect of the oxygen vacancies on the In_2O_3 surface in methanol synthesis [20,89]. It has been suggested that these vacancies are created through the heterolytic dissociation of H_2. Specifically, it involves overcoming a high H_2 activation barrier, which results in the formation of surface $OH^{\delta+}$ and $InH^{\delta-}$ species, followed by water desorption. Moreover, the generated hydride ($H^{\delta-}$) species can react with chemisorbed CO_2, forming HCOO* intermediate that can be subsequently hydrogenated to CH_3OH [90–92]. While previous studies have suggested that Ni promotion of methanol synthesis from CO_2 on In_2O_3 catalysts is mainly attributed to the low-barrier H_2 dissociation [26–28,36,74], our work offers a more comprehensive depiction of the dynamic transformations occurring during the interaction of H_2 with Ni/In_2O_3(111) model catalysts as a function of temperatures. We have observed the activation and dissociation of H_2 at the interfacial site at the molecular level. At relatively low temperatures (300–473 K), the presence of small Ni clusters facilitates H_2 activation, providing hydride (Ni-H) bonds at the Ni-In_2O_3 interface, as demonstrated by the presence of the Ni(OH)-related component in Fig. 2b. These H species play a pivotal role in generating oxygen vacancies within In_2O_3 and facilitating the hydrogenation of adsorbed surface intermediates. As temperatures rise (> 523 K), hydride coverage decreases along with the desorption of OH species (Fig. S8), followed by the creation of lattice oxygen vacancies on the oxide support. These oxygen vacancies play a crucial role in the

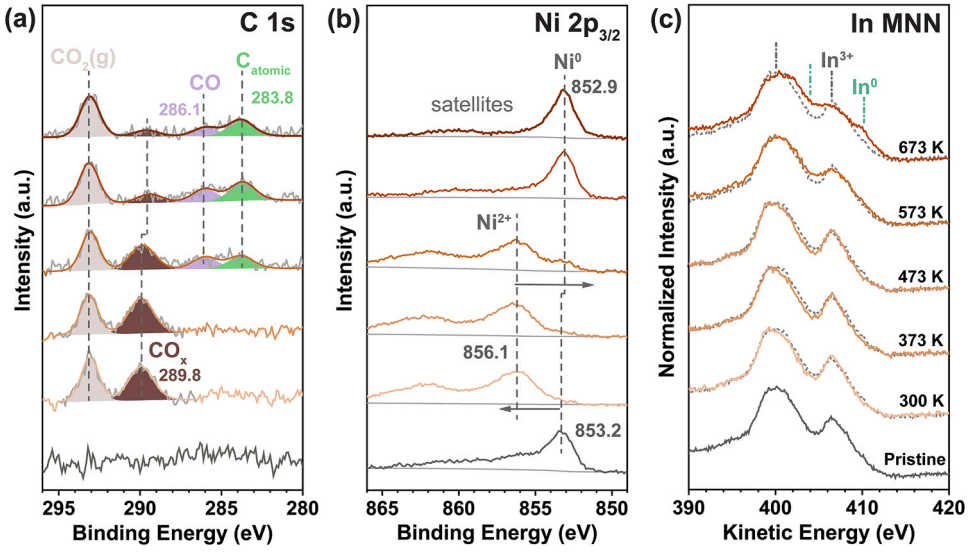

Fig. 4. NAP-XPS spectra for the Ni/In_2O_3(111) surface (θ_{Ni} ~0.50 ML) under 0.6 mbar H_2 + 0.2 mbar CO_2 at the indicated temperatures. (a) C 1 s, (b) Ni $2p_{3/2}$, and (c) In MNN. The gray dashed lines correspond to the pristine Ni/In_2O_3(111).

adsorption and hydrogenation of CO_2. Thus, it is clear that small Ni clusters on In_2O_3 substantially enhance the abundance of oxygen vacancies by facilitating H_2 dissociation, which is regarded as a critical factor that controls the overall reaction rate. However, the promoting effect of Ni on CO_2 activation should not be ignored in the context of CO_2 hydrogenation reactions.

Through careful interpretations of adsorbate chemical binding energy analysis on well-defined Ni/In_2O_3(111) surface under CO_2 hydrogenation conditions, we have indicated that H species, generated by facile H_2 dissociation on the cationic Ni site at the metal-oxide interface, readily hydrogenate CO_3* into HCOO*. Importantly, these intermediates are easily formed and desorbed without any carbon deposition during the reaction, which is the ideal characteristic of intermediates in the catalytic process. Furthermore, Cannizzaro et al. [74], employing DFT and microkinetic modeling, have demonstrated the surface coverage dynamics of the Ni_8 cluster adsorbed on In_2O_3(111), representative of small In_2O_3-supported Ni clusters. Their findings suggest a prevalence of the HCOO* + H state at lower temperatures (473 K < T < 573 K), with the oxygen vacancy state becoming dominant at higher temperatures, which is in line with our expectations based on NAP-XPS results. Additionally, they have proposed that Ni_8 clusters on stoichiometric In_2O_3(111) are involved in the hydrogenation of adsorbed CO_2 to HCOO* intermediates for CH_3OH formation, while high barriers associated with either direct or H-assisted CO activation inhibit CH_4 generation, given the exceedingly high barrier for direct C–O bond cleavage. However, it is worth noting an alternative viewpoint presented by Shen et al. [36], whose DFT simulations on Ni_4 clusters embedded in In_2O_3(111) suggest that the RWGS pathway is theoretically favored for CO_2 hydrogenation to CH_3OH synthesis. Our in-situ investigation provides additional support for the HCOO* pathway over Ni/In_2O_3 catalysts in CO_2 hydrogenation.

Our study presents new insights on the promotion effect of small Ni clusters supported on the In_2O_3(111) surface for the CO_2 hydrogenation to methanol (Fig. 5). On bare In_2O_3, the highly exothermic CO_2 reduction yields HCOO* species, subsequently hydrogenated to produce methanol. However, In_2O_3 exhibits limited H_2 activation capability, retarding the overall reaction kinetics. The addition of Ni metal promoter to In_2O_3 significantly influences the selectivity of CO_2 hydrogenation towards methanol. At the interface between the In_2O_3 and small cationic Ni clusters, electron transfer from Ni to the oxide takes place, giving rise to antibonding Ni–O and In–O couplings. Such electron transfer reduces the π back-donation from Ni to the adsorbed C-O bond, moderately weakening the Ni-C bond and consequently strengthening the C-O bond. The strong Ni-In_2O_3 interaction promotes the H_2 activation on Ni species with hydrogen spillover, along with CO_2 activation at the interfacial sites. Moreover, hydride species originating from facile H_2 dissociation on the surface contribute to the creation of oxygen vacancies, serving as active sites for the effective CO_2 activation and the hydrogenation of CO_3* to HCOO* intermediates, thus favoring the selective production of methanol. Conversely, a rapid weakening of the metal–In_2O_3 interactions occurs when larger metallic Ni nanoparticles are present. Nonetheless, there is less charge transfer at the metal–oxide interface, potentially weakening the C-O bond due to strong CO adsorption on Ni sites [93,94]. This leads to the availability of residual dissociated H atoms that readily engage in reactions with CO, hindering CH_3OH formation. Consequently, the formation of strongly bound carbon species shifts the reaction pathway towards producing CO and atomic carbon intermediates, leading to the occurrence of both the RWGS reaction and CO_2 methanation as side reactions. Furthermore, there is a risk of detrimental over-reduction of In_2O_3. Therefore, selecting the "right" metal-oxide combination and controlling the metal loading are crucial to achieve efficient CO_2 reduction while minimizing unwanted side reactions.

Our experimental results described above demonstrate that the In_2O_3(111) surface with small Ni clusters as well as surface oxygen vacancies are the active phase for CO_2 hydrogenation [27,28]. Based on the in-situ NAP-XPS studies with well-defined Ni/In_2O_3(111) model systems, we propose the following reaction steps on Ni/In_2O_3 catalysts for selective CO_2 hydrogenation to methanol: 1) activation of H_2 on Ni species with hydrogen spillover and activation of CO_2 at the metal–oxide interface, 2) H species generated on the surface cause the creation of oxygen vacancies, which serve as active sites for the effective adsorption and activation of CO_2 under the reaction temperature, 3) hydrogenation of the adsorbed CO_3* to HCOO* intermediates, 4) further hydrogenation of the intermediates to form methanol.

5. Conclusions

In conclusion, we provide a systematic investigation of the interaction between Ni and the In_2O_3(111) surface, as well as its transformations under different gas atmospheres (CO_2, H_2, and H_2/CO_2 mixtures) to elucidate the surface chemistry of the Ni/In_2O_3 catalysts during CO_2 hydrogenation. The results highlight the crucial role of metal-support interactions in determining the chemical and structural properties of Ni/In_2O_3(111) model catalysts. At low Ni coverages (< 0.2 ML), small cationic Ni clusters exhibit strong interactions with the oxide surface. As the Ni coverage increases beyond 0.3 ML, the Ni adatoms gradually recover their metallic character, leading to the formation of large clusters and three-dimensional nanoparticles. On stoichiometric In_2O_3(111), interfacial cationic Ni species experience electronic perturbations that facilitate CO_2 activation and H_2 dissociation. The generated oxygen vacancies through facile H_2 splitting contribute to CO_2 adsorption and the hydrogenation of CO_3* to HCOO* intermediates, promoting the selective formation of methanol. Conversely, at higher Ni coverages with larger particles, the novel chemical behavior of the metal disappears due to weakened metal-support interactions. The presence of metallic Ni nanoparticles considerably enhances H_2 and CO_2 activation. Nonetheless, the formation of strongly bound carbon species shifts the reaction pathway towards the production of CO and atomic carbon intermediates, leading to the

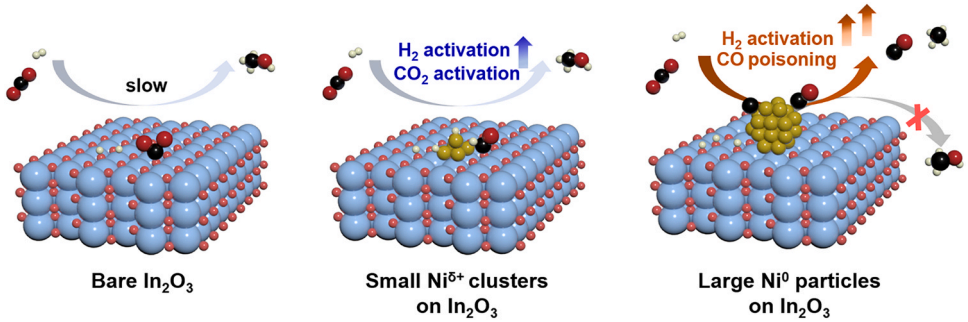

Fig. 5. Illustration of the effects of Ni promoter on In_2O_3 during CO_2 hydrogenation. The In, O, Ni and C atoms are colored in blue, red, yellow and black, respectively.

occurrence of both side reactions: RWGS and CO_2 methanation. Our study provides experimental understandings of the reaction mechanism for the Ni/In_2O_3 catalysts in CO_2 hydrogenation, which offers insights into metal-support interactions, reaction intermediates, and metal loading effects for the rational design of advanced metal promoter-In_2O_3 catalysts.

CRediT authorship contribution statement

Yishui Ding: Investigation, Conceptualization, Formal analysis, Visualization, Writing – original draft. **Jie Chen:** Investigation, Formal analysis, Visualization, Writing – review & editing. **Xu Lian:** Conceptualization, Methodology, Formal analysis, Writing – review & editing. **Zhangliu Tian:** Resources, Writing – review & editing. **Xiangrui Geng:** Formal analysis, Writing – review & editing. **Yihe Wang:** Formal analysis, Writing – review & editing. **Yuan Liu:** Validation, Writing – review & editing. **Wei Wang**: Writing – review & editing. **Meng Wang:** Resources, Visualization. **Yukun Xiao:** Investigation. **Tengyu Jin:** Resources. **Mingyue Sun**: Investigation. **Zhenni Yang:** Resources. **Kelvin H. L. Zhang:** Resources, Supervision. **Jian-Qiang Zhong:** Formal analysis, Data curation, Supervision, Writing – review & editing. **Wei Chen:** Conceptualization, Data curation, Writing – review & editing, Supervision, Project administration, Funding acquisition.

Declaration of Competing Interest

The authors declare that they have no known competing financial interests or personal relationships that could have appeared to influence the work reported in this paper.

Data availability

Data will be made available on request.

Acknowledgments

Authors acknowledge financial support from the National Research Foundation, Singapore, and A*STAR (Agency for Science, Technology and Research) under its LCER FI program Award No U2102d2002, and the National Science Foundation of China (Grant No. 22002031).

Appendix A. Supporting information

Supplementary data associated with this article can be found in the online version at DOI:10.1016/j.apcatb.2023.123508.

References

[1] T.R. Karl, K.E. Trenberth, Modern global climate change, Science 302 (2003) 1719–1723.
[2] J. Artz, T.E. Müller, K. Thenert, J. Kleinekorte, R. Meys, A. Sternberg, A. Bardow, W. Leitner, Sustainable conversion of carbon dioxide: an integrated review of catalysis and life cycle assessment, Chem. Rev. 118 (2018) 434–504.
[3] S.C. Doney, V.J. Fabry, R.A. Feely, J.A. Kleypas, Ocean acidification: the other CO_2 problem, Annu. Rev. Mar. Sci. 1 (2009) 169–192.
[4] N. Mac Dowell, P.S. Fennell, N. Shah, G.C. Maitland, The role of CO_2 capture and utilization in mitigating climate change, Nat. Clim. Change 7 (2017) 243–249.
[5] M. Bui, C.S. Adjiman, A. Bardow, E.J. Anthony, A. Boston, S. Brown, P.S. Fennell, S. Fuss, A. Galindo, L.A. Hackett, Carbon capture and storage (CCS): the way forward, Energy Environ. Sci. 11 (2018) 1062–1176.
[6] K. Lee, U. Anjum, T.P. Araújo, C. Mondelli, Q. He, S. Furukawa, J. Pérez-Ramírez, S.M. Kozlov, N. Yan, Atomic Pd-promoted $ZnZrO_x$ solid solution catalyst for CO_2 hydrogenation to methanol, Appl. Catal. B 304 (2022), 120994.
[7] D. Masih, S. Rohani, J.N. Kondo, T. Tatsumi, Low-temperature methanol dehydration to dimethyl ether over various small-pore zeolites, Appl. Catal. B 217 (2017) 247–255.
[8] E. Catizzone, S.V. Daele, M. Bianco, A. Di Michele, A. Aloise, M. Migliori, V. Valtchev, G. Giordano, Catalytic application of ferrierite nanocrystals in vapour-phase dehydration of methanol to dimethyl ether, Appl. Catal. B 243 (2019) 273–282.
[9] J. Zhong, X. Yang, Z. Wu, B. Liang, Y. Huang, T. Zhang, State of the art and perspectives in heterogeneous catalysis of CO_2 hydrogenation to methanol, Chem. Soc. Rev. 49 (2020) 1385–1413.
[10] J. Wang, G. Li, Z. Li, C. Tang, Z. Feng, H. An, H. Liu, T. Liu, C. Li, A highly selective and stable ZnO-ZrO_2 solid solution catalyst for CO_2 hydrogenation to methanol, Sci. Adv. 3 (2017), e1701290.
[11] Y. Yan, R.J. Wong, Z. Ma, F. Donat, S. Xi, S. Saqline, Q. Fan, Y. Du, A. Borgna, Q. He, CO_2 hydrogenation to methanol on tungsten-doped Cu/CeO_2 catalysts, Appl. Catal. B 306 (2022), 121098.
[12] X. Jiang, X. Nie, X. Guo, C. Song, J.G. Chen, Recent advances in carbon dioxide hydrogenation to methanol via heterogeneous catalysis, Chem. Rev. 120 (2020) 7984–8034.
[13] N.J. Divins, D. Kordus, J. Timoshenko, I. Sinev, I. Zegkinoglou, A. Bergmann, S. W. Chee, S. Widrinna, O. Karslıoğlu, H. Mistry, M. Lopez Luna, J.Q. Zhong, A. S. Hoffman, A. Boubnov, J.A. Boscoboinik, M. Heggen, R.E. Dunin-Borkowski, S. R. Bare, B.R. Cuenya, Operando high-pressure investigation of size-controlled CuZn catalysts for the methanol synthesis reaction, Nat. Commun. 12 (2021) 1435.
[14] J. Sehested, Industrial and scientific directions of methanol catalyst development, J. Catal. 371 (2019) 368–375.
[15] S. Kuld, M. Thorhauge, H. Falsig, C.F. Elkjær, S. Helveg, I. Chorkendorff, J. Sehested, Quantifying the promotion of Cu catalysts by ZnO for methanol synthesis, Science 352 (2016) 969–974.
[16] W. Wang, S. Wang, X. Ma, J. Gong, Recent advances in catalytic hydrogenation of carbon dioxide, Chem. Soc. Rev. 40 (2011) 3703–3727.
[17] O. Martin, A.J. Martín, C. Mondelli, S. Mitchell, T.F. Segawa, R. Hauert, C. Drouilly, D. Curulla-Ferré, J. Pérez-Ramírez, Indium oxide as a superior catalyst for methanol synthesis by CO_2 hydrogenation, Angew. Chem. Int. Ed. 128 (2016) 6369–6373.
[18] S. Dang, B. Qin, Y. Yang, H. Wang, J. Cai, Y. Han, S. Li, P. Gao, Y. Sun, Rationally designed indium oxide catalysts for CO_2 hydrogenation to methanol with high activity and selectivity, Sci. Adv. 6 (2020), eaaz2060.
[19] J. Wang, G. Zhang, J. Zhu, X. Zhang, F. Ding, A. Zhang, X. Guo, C. Song, CO_2 hydrogenation to methanol over In_2O_3-based catalysts: from mechanism to catalyst development, ACS Catal. 11 (2021) 1406–1423.
[20] M.S. Frei, M. Capdevila-Cortada, R. García-Muelas, C. Mondelli, N. López, J. A. Stewart, D.C. Ferré, J. Perez-Ramirez, Mechanism and microkinetics of methanol synthesis via CO_2 hydrogenation on indium oxide, J. Catal. 361 (2018) 313–321.
[21] J. Ye, C. Liu, D. Mei, Q. Ge, Active oxygen vacancy site for methanol synthesis from CO_2 hydrogenation on In_2O_3 (110): a DFT study, ACS Catal. 3 (2013) 1296–1306.
[22] A. Cao, Z. Wang, H. Li, J.K. Nørskov, Relations between surface oxygen vacancies and activity of methanol formation from CO_2 hydrogenation over In_2O_3 surfaces, ACS Catal. 11 (2021) 1780–1786.
[23] M.S. Frei, C. Mondelli, R. García-Muelas, K.S. Kley, B. Puértolas, N. López, O. V. Safonova, J.A. Stewart, D. Curulla Ferré, J. Pérez-Ramírez, Atomic-scale engineering of indium oxide promotion by palladium for methanol production via CO_2 hydrogenation, Nat. Commun. 10 (2019) 3377.
[24] N. Rui, Z. Wang, K. Sun, J. Ye, Q. Ge, C.-j Liu, CO_2 hydrogenation to methanol over Pd/In_2O_3: effects of Pd and oxygen vacancy, Appl. Catal. B 218 (2017) 488–497.
[25] T. Pinheiro Araujo, J. Morales-Vidal, T. Zou, R. García-Muelas, P.O. Willi, K. M. Engel, O.V. Safonova, D. Faust Akl, F. Krumeich, R.N. Grass, Flame spray pyrolysis as a synthesis platform to assess metal promotion in In_2O_3-catalyzed CO_2 hydrogenation, Adv. Energy Mater. 12 (2022), 2103707.
[26] M.S. Frei, C. Mondelli, R. García-Muelas, J. Morales-Vidal, M. Philipp, O. V. Safonova, N. López, J.A. Stewart, D.C. Ferré, J. Pérez-Ramírez, Nanostructure of nickel-promoted indium oxide catalysts drives selectivity in CO_2 hydrogenation, Nat. Commun. 12 (2021) 1960.
[27] J. Zhu, F. Cannizzaro, L. Liu, H. Zhang, N. Kosinov, I.A. Filot, J. Rabeah, A. Brückner, E.J. Hensen, Ni–In synergy in CO_2 hydrogenation to methanol, ACS Catal. 11 (2021) 11371–11384.
[28] X. Jia, K. Sun, J. Wang, C. Shen, C.-j Liu, Selective hydrogenation of CO_2 to methanol over Ni/In_2O_3 catalyst, J. Energy Chem. 50 (2020) 409–415.
[29] K. Sun, C. Shen, R. Zou, C.-j Liu, Highly active Pt/In_2O_3-ZrO_2 catalyst for CO_2 hydrogenation to methanol with enhanced CO tolerance: the effects of ZrO_2, Appl. Catal. B 320 (2023), 122018.
[30] Z. Han, C. Tang, J. Wang, L. Li, C. Li, Atomically dispersed Pt^{n+} species as highly active sites in Pt/In2O3 catalysts for methanol synthesis from CO2 hydrogenation, J. Catal. 394 (2021) 236–244.
[31] J. Wang, K. Sun, X. Jia, C.-j Liu, CO_2 hydrogenation to methanol over Rh/In_2O_3 catalyst, Catal. Today 365 (2021) 341–347.
[32] N.H.M. Dostagir, C. Thompson, H. Kobayashi, A.M. Karim, A. Fukuoka, A. Shrotri, Rh promoted In_2O_3 as a highly active catalyst for CO_2 hydrogenation to methanol, Catal. Sci. Technol. 10 (2020) 8196–8202.
[33] N. Rui, F. Zhang, K. Sun, Z. Liu, W. Xu, E. Stavitski, S.D. Senanayake, J. A. Rodriguez, C.-J. Liu, Hydrogenation of CO_2 to methanol on a $Au^{\delta+}$–In_2O_{3-x} catalyst, ACS Catal. 10 (2020) 11307–11317.
[34] C. Shen, K. Sun, R. Zou, Q. Wu, D. Mei, C.-j Liu, CO_2 Hydrogenation to methanol on indium oxide-supported rhenium catalysts: the effects of size, ACS Catal. 12 (2022) 12658–12669.
[35] N. Rui, K. Sun, C. Shen, C.-J. Liu, Density functional theoretical study of Au_4/In_2O_3 catalyst for CO_2 hydrogenation to methanol: the strong metal-support interaction and its effect, J. CO_2 Util. 42 (2020), 101313.
[36] C. Shen, Q. Bao, W. Xue, K. Sun, Z. Zhang, X. Jia, D. Mei, C.-j Liu, Synergistic effect of the metal-support interaction and interfacial oxygen vacancy for CO_2 hydrogenation to methanol over Ni/In_2O_3 catalyst: a theoretical study, J. Energy Chem. 65 (2022) 623–629.

[37] K. Sun, N. Rui, C. Shen, C.-j Liu, Theoretical study of selective hydrogenation of CO_2 to methanol over Pt_4/In_2O_3 model catalyst, J. Phys. Chem. C 125 (2021) 10926–10936.

[38] J.L. Snider, V. Streibel, M.A. Hubert, T.S. Choksi, E. Valle, D.C. Upham, J. Schumann, M.S. Duyar, A. Gallo, F. Abild-Pedersen, Revealing the synergy between oxide and alloy phases on the performance of bimetallic In–Pd catalysts for CO_2 hydrogenation to methanol, ACS Catal. 9 (2019) 3399–3412.

[39] A. García-Trenco, A. Regoutz, E.R. White, D.J. Payne, M.S. Shaffer, C.K. Williams, PdIn intermetallic nanoparticles for the hydrogenation of CO_2 to methanol, Appl. Catal. B 220 (2018) 9–18.

[40] Z. Shi, Q. Tan, C. Tian, Y. Pan, X. Sun, J. Zhang, D. Wu, CO_2 hydrogenation to methanol over Cu-In intermetallic catalysts: effect of reduction temperature, J. Catal. 379 (2019) 78–89.

[41] L. Yao, X. Shen, Y. Pan, Z. Peng, Synergy between active sites of Cu-In-Zr-O catalyst in CO_2 hydrogenation to methanol, J. Catal. 372 (2019) 74–85.

[42] X. Lian, J. Gao, Y. Ding, Y. Liu, W. Chen, Unraveling catalytic reaction mechanism by in situ near ambient pressure X-ray photoelectron spectroscopy, J. Phys. Chem. Lett. 13 (2022) 8264–8277.

[43] J. Dou, Z. Sun, A.A. Opalade, N. Wang, W. Fu, F.F. Tao, Operando chemistry of catalyst surfaces during catalysis, Chem. Soc. Rev. 46 (2017) 2001–2027.

[44] J.-Q. Zhong, S. Shaikhutdinov, B. Roldan, Cuenya, structural evolution of Ga–Cu model catalysts for CO_2 hydrogenation reactions, J. Phys. Chem. C 125 (2021) 1361–1367.

[45] K. Pussi, A. Matilainen, V.R. Dhanak, A. Walsh, R.G. Egdell, K.H.L. Zhang, Surface structure of $In_2O_3(111)$ (1×1) determined by density functional theory calculations and low energy electron diffraction, Surf. Sci. 606 (2012) 1–6.

[46] D.W. Davies, A. Walsh, J.J. Mudd, C.F. McConville, A. Regoutz, J.M. Kahk, D. J. Payne, V.R. Dhanak, D. Hesp, K. Pussi, Identification of lone-pair surface states on indium oxide, J. Phys. Chem. C 123 (2018) 1700–1709.

[47] K. Zhang, D. Payne, R. Palgrave, V. Lazarov, W. Chen, A. Wee, C. McConville, P. King, T. Veal, G. Panaccione, Surface structure and electronic properties of $In_2O_3(111)$ single-crystal thin films grown on Y-stabilized $ZrO_2(111)$, Chem. Mater. 21 (2009) 4353–4355.

[48] K. Zhang, R. Egdell, F. Offi, S. Iacobucci, L. Petaccia, S. Gorovikov, P. King, Microscopic origin of electron accumulation in In_2O_3, Phys. Rev. Lett. 110 (2013), 056803.

[49] K. Yuan, J.-Q. Zhong, S. Sun, Y. Ren, J.L. Zhang, W. Chen, Reactive intermediates or inert graphene? temperature-and pressure-determined evolution of carbon in the CH_4–Ni (111) system, ACS Catal. 7 (2017) 6028–6037.

[50] Z. Ma, X. Lian, K. Yuan, S. Sun, C. Gu, J.L. Zhang, J. Lyu, J.-Q. Zhong, L. Liu, H. Li, Pressure-dependent band-bending in ZnO: a near-ambient-pressure X-ray photoelectron spectroscopy study, J. Energy Chem. 60 (2021) 25–31.

[51] X. Zhou, Q. Shen, K. Yuan, W. Yang, Q. Chen, Z. Geng, J. Zhang, X. Shao, W. Chen, G. Xu, X. Yang, K. Wu, Unraveling charge state of supported Au single-atoms during CO oxidation, J. Am. Chem. Soc. 140 (2018) 554–557.

[52] J.-Q. Zhong, X. Zhou, K. Yuan, C.A. Wright, A. Tadich, D. Qi, H.X. Li, K. Wu, G. Q. Xu, W. Chen, Probing the effect of the Pt–Ni–Pt (111) bimetallic surface electronic structures on the ammonia decomposition reaction, Nanoscale 9 (2017) 666–672.

[53] M. Wagner, S. Seiler, B. Meyer, L.A. Boatner, M. Schmid, U. Diebold, Reducing the $In_2O_3(111)$ surface results in ordered indium adatoms, Adv. Mater. Interfaces 1 (2014), 1400289.

[54] D.E. Gordon, R.M. Lambert, CO_2 adsorption on oxygen-modified Ni(111), Surf. Sci. 287 (1993) 114–118.

[55] J. Carrasco, D. López-Durán, Z. Liu, T. Duchoň, J. Evans, S.D. Senanayake, E. J. Crumlin, V. Matolín, J.A. Rodríguez, M.V. Ganduglia-Pirovano, In situ and theoretical studies for the dissociation of water on an active Ni/CeO_2 catalyst: importance of strong metal–support interactions for the cleavage of O–H bonds, Angew. Chem. Int. Ed. 54 (2015) 3917–3921.

[56] F. Zhang, R.A. Gutiérrez, P.G. Lustemberg, Z. Liu, N. Rui, T. Wu, P.J. Ramírez, W. Xu, H. Idriss, M.V. Ganduglia-Pirovano, Metal–support interactions and C1 chemistry: transforming Pt-CeO_2 into a highly active and stable catalyst for the conversion of carbon dioxide and methane, ACS Catal. 11 (2021) 1613–1623.

[57] M. Bäumer, H.-J. Freund, Metal deposits on well-ordered oxide films, Prog. Surf. Sci. 61 (1999) 127–198.

[58] A. Bruix, J.A. Rodriguez, P.J. Ramírez, S.D. Senanayake, J. Evans, J.B. Park, D. Stacchiola, P. Liu, J. Hrbek, F. Illas, A. New, Type of strong metal–support interaction and the production of H_2 through the transformation of water on Pt/$CeO_2(111)$ and Pt/$CeO_x/TiO_2(110)$ catalysts, J. Am. Chem. Soc. 134 (2012) 8968–8974.

[59] Z. Mao, P.G. Lustemberg, J.R. Rumptz, M.V. Ganduglia-Pirovano, C.T. Campbell, Ni nanoparticles on $CeO_2(111)$: energetics, electron transfer, and structure by Ni adsorption calorimetry, spectroscopies, and density functional theory, ACS Catal. 10 (2020) 5101–5114.

[60] Z. Liu, D.C. Grinter, P.G. Lustemberg, T.D. Nguyen-Phan, Y. Zhou, S. Luo, I. Waluyo, E.J. Crumlin, D.J. Stacchiola, J. Zhou, Dry reforming of methane on a highly-active Ni-CeO_2 catalyst: effects of metal-support interactions on C− H bond breaking, Angew. Chem. Int. Ed. 55 (2016) 7455–7459.

[61] Y. Zhou, J. Zhou, Interactions of Ni nanoparticles with reducible $CeO_2(111)$ thin films, J. Phys. Chem. C 116 (2012) 9544–9549.

[62] M. Wagner, P. Lackner, S. Seiler, S. Gerhold, J. Osiecki, K. Schulte, L.A. Boatner, M. Schmid, B. Meyer, U. Diebold, Well-ordered In adatoms at the $In_2O_3(111)$ surface created by Fe deposition, Phys. Rev. Lett. 117 (2016), 206101.

[63] M. Roiaz, E. Monachino, C. Dri, M. Greiner, A. Knop-Gericke, R. Schlögl, G. Comelli, E. Vesselli, Reverse water–gas shift or sabatier methanation on Ni (110)? stable surface species at near-ambient pressure, J. Am. Chem. Soc. 138 (2016) 4146–4154.

[64] C. Heine, B.A. Lechner, H. Bluhm, M. Salmeron, Recycling of CO_2: probing the chemical state of the Ni (111) surface during the methanation reaction with ambient-pressure X-ray photoelectron spectroscopy, J. Am. Chem. Soc. 138 (2016) 13246–13252.

[65] M. Li, W. Luo, A. Züttel, Near ambient-pressure X-ray photoelectron spectroscopy study of CO_2 activation and hydrogenation on indium/copper surface, J. Catal. 395 (2021) 315–324.

[66] V. Brinzari, B.K. Cho, G. Korotcenkov, Carbon 1s photoemission line analysis of C-based adsorbate on $(111)In_2O_3$ surface: the influence of reducing and oxidizing conditions, Appl. Surf. Sci. 390 (2016) 897–902.

[67] J. Ye, C. Liu, Q. Ge, DFT study of CO_2 adsorption and hydrogenation on the In_2O_3 surface, J. Phys. Chem. C 116 (2012) 7817–7825.

[68] U. Burghaus, Surface chemistry of CO_2–adsorption of carbon dioxide on clean surfaces at ultrahigh vacuum, Prog. Surf. Sci. 89 (2014) 161–217.

[69] Y. Ren, C. Xin, Z. Hao, H. Sun, S.L. Bernasek, W. Chen, G.Q. Xu, Probing the reaction mechanism in CO_2 hydrogenation on bimetallic Ni/Cu(100) with near-ambient pressure X-Ray photoelectron spectroscopy, ACS Appl. Mater. Interfaces 12 (2019) 2548–2554.

[70] K. Yuan, J.-Q. Zhong, X. Zhou, L. Xu, S.L. Bergman, K. Wu, G.Q. Xu, S.L. Bernasek, H.X. Li, W. Chen, Dynamic oxygen on surface: catalytic intermediate and coking barrier in the modeled CO_2 reforming of CH_4 on Ni (111), ACS Catal. 6 (2016) 4330–4339.

[71] Y. Zang, J. Cai, Y. Han, H. Wu, W. Zhu, S. Shi, H. Zhang, Y. Ran, F. Yang, M. Ye, CO_2 activation on Ni (111) and Ni (110) surfaces in the presence of hydrogen, J. Phys. Chem. Lett. 14 (2023) 4381–4387.

[72] H. Chen, M.A. Blatnik, C.L. Ritterhoff, I. Sokolović, F. Mirabella, G. Franceschi, M. Riva, M. Schmid, J. Čechal, B. Meyer, U. Diebold, M. Wagner, Water structures reveal local hydrophobicity on the $In_2O_3(111)$ surface, ACS Nano 16 (2022) 21163–21173.

[73] N. Weidler, J. Schuch, F. Knaus, P. Stenner, S. Hoch, A. Maljusch, R. Schäfer, B. Kaiser, W. Jaegermann, X-ray photoelectron spectroscopic investigation of plasma-enhanced chemical vapor deposited NiO_x, $NiO_x(OH)_y$, and $CoNiO_x(OH)_y$: influence of the chemical composition on the catalytic activity for the oxygen evolution reaction, J. Phys. Chem. C 121 (2017) 6455–6463.

[74] F. Cannizzaro, E.J. Hensen, I.A. Filot, The promoting role of Ni on In_2O_3 for CO_2 hydrogenation to methanol, ACS Catal. 13 (2023) 1875–1892.

[75] H. Idriss, On the wrong assignment of the XPS O1s signal at 531–532 eV attributed to oxygen vacancies in photo- and electro-catalysts for water splitting and other materials applications, Surf. Sci. 712 (2021), 121894.

[76] A. Posada-Borbon, H. Grönbeck, Hydrogen adsorption on $In_2O_3(111)$ and $In_2O_3(110)$, Phys. Chem. Chem. Phys. 22 (2020) 16193–16202.

[77] A. Posada-Borbón, N. Bosio, H. Grönbeck, On the signatures of oxygen vacancies in O 1s core level shifts, Surf. Sci. 705 (2021), 121761.

[78] S.D. Senanayake, P.J. Ramírez, I. Waluyo, S. Kundu, K. Mudiyanselage, Z. Liu, Z. Liu, S. Axnanda, D.J. Stacchiola, J. Evans, J.A. Rodriguez, Hydrogenation of CO_2 to methanol on $CeO_x/Cu(111)$ and $ZnO/Cu(111)$ catalysts: role of the metal–oxide interface and importance of Ce^{3+} sites, J. Phys. Chem. C 120 (2016) 1778–1784.

[79] P. Amann, B. Klötzer, D. Degerman, N. Köpfle, T. Götsch, P. Lömker, C. Rameshan, K. Ploner, D. Bikaljevic, H.-Y. Wang, The state of zinc in methanol synthesis over a Zn/ZnO/Cu (211) model catalyst, Science 376 (2022) 603–608.

[80] C. Au, W. Hirsch, W. Hirschwald, Adsorption and interaction of carbon dioxide, formic acid and hydrogen/carbon dioxide mixtures on (1010) zinc oxide surfaces studied by photoelectron spectroscopy (XPS and UPS), Surf. Sci. 199 (1988) 507–517.

[81] P. Gao, S. Li, X. Bu, S. Dang, Z. Liu, H. Wang, L. Zhong, M. Qiu, C. Yang, J. Cai, Direct conversion of CO_2 into liquid fuels with high selectivity over a bifunctional catalyst, Nat. Chem. 9 (2017) 1019–1024.

[82] A. Tsoukalou, P.M. Abdala, D. Stoian, X. Huang, M.-G. Willinger, A. Fedorov, C. R. Müller, Structural evolution and dynamics of an In_2O_3 catalyst for CO_2 hydrogenation to methanol: an operando XAS-XRD and in situ TEM study, J. Am. Chem. Soc. 141 (2019) 13497–13505.

[83] M. Seah, I. Gilmore, S. Spencer, Quantitative XPS: I. Analysis of X-ray photoelectron intensities from elemental data in a digital photoelectron database, J. Electron Spectrosc. Relat. Phenom. 120 (2001) 93–111.

[84] S.D. Senanayake, J. Evans, S. Agnoli, L. Barrio, T.-L. Chen, J. Hrbek, J. A. Rodriguez, Water–gas shift and CO methanation reactions over Ni–$CeO_2(111)$ catalysts, Top. Catal. 54 (2011) 34–41.

[85] J. Cai, Y. Han, S. Chen, E.J. Crumlin, B. Yang, Y. Li, Z. Liu, CO_2 activation on Ni (111) and Ni(100) surfaces in the presence of H_2O: an ambient-pressure X-ray photoelectron spectroscopy study, J. Phys. Chem. C 123 (2019) 12176–12182.

[86] S.-G. Wang, D.-B. Cao, Y.-W. Li, J. Wang, H. Jiao, Chemisorption of CO_2 on nickel surfaces, J. Phys. Chem. B 109 (2005) 18956–18963.

[87] J. Ren, H. Guo, J. Yang, Z. Qin, J. Lin, Z. Li, Insights into the mechanisms of CO_2 methanation on Ni(111) surfaces by density functional theory, Appl. Surf. Sci. 351 (2015) 504–516.

[88] P.G. Lustemberg, P.J. Ramírez, Z. Liu, R.A. Gutierrez, D.G. Grinter, J. Carrasco, S. D. Senanayake, J.A. Rodriguez, M.V. Ganduglia-Pirovano, Room-temperature activation of methane and dry re-forming with CO_2 on Ni-$CeO_2(111)$ surfaces: effect of Ce^{3+} sites and metal–support interactions on C–H bond cleavage, ACS Catal. 6 (2016) 8184–8191.

[89] B. Qin, S. Li, First principles investigation of dissociative adsorption of H_2 during CO_2 hydrogenation over cubic and hexagonal In_2O_3 catalysts, Phys. Chem. Chem. Phys. 22 (2020) 3390–3399.

[90] T.-y Chen, C. Cao, T.-b Chen, X. Ding, H. Huang, L. Shen, X. Cao, M. Zhu, J. Xu, J. Gao, Unraveling highly tunable selectivity in CO_2 hydrogenation over bimetallic In-Zr oxide catalysts, ACS Catal. 9 (2019) 8785–8797.
[91] C. Yang, C. Pei, R. Luo, S. Liu, Y. Wang, Z. Wang, Z.-J. Zhao, J. Gong, Strong electronic oxide–support interaction over In_2O_3/ZrO_2 for highly selective CO_2 hydrogenation to methanol, J. Am. Chem. Soc. 142 (2020) 19523–19531.
[92] J. Ye, C.-j Liu, D. Mei, Q. Ge, Methanol synthesis from CO_2 hydrogenation over a Pd_4/In_2O_3 model catalyst: a combined DFT and kinetic study, J. Catal. 317 (2014) 44–53.
[93] M.-M. Millet, G. Algara-Siller, S. Wrabetz, A. Mazheika, F. Girgsdies, D. Teschner, F. Seitz, A. Tarasov, S.V. Levchenko, R. Schlögl, Ni single atom catalysts for CO_2 activation, J. Am. Chem. Soc. 141 (2019) 2451–2461.
[94] X. Li, J. Lin, L. Li, Y. Huang, X. Pan, S.E. Collins, Y. Ren, Y. Su, L. Kang, X. Liu, Controlling CO_2 hydrogenation selectivity by metal-supported electron transfer, Angew. Chem. Int. Ed. 59 (2020) 19983–19989.